DEVELOPMENT OF MODELS TO ESTIMATE EMI FROM SWITCHED-MODE POWER SUPPLY
Part I/II

by

Gian Lorenzo Giuliattini Burbui

A DISSERTATION

Presented to the

UNIVERSITY OF BOLOGNA

In Partial Fulfillment of the Requirements for the Degree

DOCTOR OF PHILOSOPHY
in
ELECTRICAL ENGINEERING

2006

ABSTRACT

This dissertation describes algorithms and techniques developed at the University of Bologna to estimate radiated EMI from Switched-Mode Power Supply (SMPS) .

The first chapter presents some basic ideas when dealing with radiated EMI from SMPS and briefly describes the principal sources of EMI.

The second chapter describes the theory, the construction and calibration of an optically-linked triple loop antenna system (TLS) to measure electric and magnetic field from SMPS. The TLA has been built and calibrated in the EMC laboratory of the University of Bologna. The TLS is used as reference receiver and to validate the proposed model.

The third chapeter presents a resistance-inductance-capacitance (RLC) model for estimating current waveforms in digital CMOS circuits. The model is based on parameters that are readily derived from information available in board layout files and component data sheets or IBIS files. Compared with the simpler triangular waveform traditionally used to approximate current in CMOS circuits, the RLC model more accurately estimates the shape of the current waveform in the time domain and the amplitudes of the upper harmonics in the frequency domain. This chapter has been developed in collaboration with Dr. Todd H. Hubing and Yan Fu at the University of Missouri-Rolla and submitted for pubblication to IEEE Tansaction on Electromagnetic Compatibility.

The fourth chapter describes an algorithm based on analytical formulas to estimate radiated EMI from SMPS. The model is based on parameters that are readily derived from information available in board layout files, component data sheets and geometry dimensions. The EMI voltage and current noise sources are described by simple models: the trapezoidal waveform model and the RLC model presented in the previous chapter. The electric and magnetic coupling mechanisms between the sources and the victim are described by equivalent circuits. Their validation is pursued by using the TLS.

The last chapter describes the application of the proposed model to a commercial SMPS for personal computer. The proposed model shows a very good agreement with measurements.

ACKNOWLEDGMENTS

I would like to express my sincere gratitude to Prof. Ing. Ugo Reggiani my graduate advisor, for valuable discussions and direction during my pursuit of Ph.D. degree at University of Bologna. I learned most aspects of doing research activity, presenting and publishing my work from my advisor. I would also like to thank to Dr. Leonardo Sandrolini for his helpful discussions and instructions. Special thanks to Dr. Todd H. Hubing for his teaching in classes and beneficial discussions regarding research activity at the University of Missouri-Rolla. It is a pleasure to acknowledge all the students in the UMR-EMC lab, Andrea Albertini technicians of the University of Bologna for their support and teamwork.

I am most appreciative to my wife Costanza for supporting me these three years and especially during the period I spent at the University of Missouri-Rolla.

Contents

Equation Chapter 1 Section 1Chapter 1

I. INTRODUCTION

Since their introduction at the end of 1960s, switched mode power supplies (SMPS) has become more and more popular, being used in the majority of today's electronic and electric equipment. As regard as EMI, SMPS have always been a serious concern, because of both conducted and radiated emissions. This first former has been covered extensively in [1], while the latter has a less estense reference [2]. Particularly, the "radiated emissions" in the low frequency range (9 kHz – 30 MHz) has not been looked into deeply.

The noise energy can be transferred from one location (source) to another (receiver) by four different mechanisms [8]:

1. conduction on wires;
2. electromagnetic wave radiation;
3. magnetic fields;
4. electric fields.

All noise problems involve at least one of these mechanisms.

Conductive mechanism or common impedance coupling requires at least two contacts (metal wires or occasionally non metal conductors) between the noise source and the susceptible circuit; one to carries the noise current from the source to the receiver and the other to returns the noise current to its source.

The electromagnetic wave radiation produced by an antenna can be a dominant effect when the distance between the noise source and the susceptible receiver are grather than the wavelength of the source. The magnetic coupling mechanism is related to time changing current of the source, whereas, the electric coupling mechanism is related to time voltage changing in the source. For high impedance values of the load the electric mechanism is dominant while for low impedance value of the load the magnetic mechanism is dominant [3].

The noise from SMPS is due to two different kinds of sources:

1. switching power modules,
2. control circuit logic.

Regarding to switching power modules, the fundamental switching frequency of the majority today commercial available SMPS lie within the 10 kHz to 500 kHz range whereas the

maximum frequency with a significant amplitude comparing to the fundamental frequency for EMI purpose is determined by the smallest rise time in the circuit and can be computed using

$$f_{\max} = \frac{10}{\pi t_r} \tag{1.1}$$

For SMPS the smallest rise time referring to the power side is in the order of 100 ns; there fore the maximum frequency of interest for EMC should be in the order of 30 MHz. Therefore noise sources from switching power modules are in the 9 kHz-30 MHz frequency range.

For this frequency range the cables attached to a SMPS are not efficient antennas [4]. The efficiency of the antenna are due to:

1. reflection because of the mismatch between the transmission line and the antenna,
2. conduction and dielectric losses in the antenna.

$$e_0 = e_c e_d e_r \tag{1.2}$$

being $e_r = 1 - \left|\frac{Z_{in} - Z_C}{Z_{in} + Z_C}\right|^2$ the reflection efficiency, e_c and e_d conduction and dielectric efficiency of the antenna respectively.

For a infinitesimal dipole ($L<<\lambda$) the input resistance is about the radiation resistance of the cable $R_{in} \approx R_{rad} = 0.3\ \Omega$ and it presents a very large mismatch when connected to 50-75 Ω transmission lines. The reflection efficiency and hence the overall efficiency is very small.

For very short antenna the boundary between reactive near-field region and far-field region is $\frac{\lambda}{2\pi}$, for the 9kHz-30 MHz range the respectively wavelength λ is in the 33 km-10 m and this boundary distance is 5.2 km-1.60 m.

Therefore any susceptible receiver not connected to the source and far less than 1.6 m from the SMPS needs to be considered in the reactive near-field region. Therefore the noise energy, getting out of the SMPS, is coupled electrically or magnetically to the susceptible receiver.

Principal EMI sources of a SMPS are [2]:

1. The time varying current in the primary loop that comprises the switching transistor, the transformer or the storage inductor and the primary capacitor.
2. The time varying current in the secondary loop comprise the transformer secondary, the rectifiers, the inductor and the load.

3. The time varying voltage between the heatsinks and ground reference
4. The transformer leakage field especially during current peaks
5. Filter inductors that can convert some of the reactive power into radiated EMI unless packaged carefully.

Few papers present models to estimate EMI emissions in SMPS [5-7], considering the effect of trace geometry, heatsinks and other parameters.

For electric/electronic equipment, which radiated emissions are in the 30 MHz-1 GHz range, the PCB EMI Expert System developed at the University of Missouri-Rolla can be very useful to estimate the radiated emissions and to deeply understand the sources and the mechanisms of electromagnetic radiations [9-13].

Chapter 2

A Triple Loop Antenna System for Electric and Magnetic-Field Measurement

I. INTRODUCTION

At frequencies lower than 30 MHz rules and regulations [1,2] always refer to the magnetic field strength measured in an OATS (Open Area Test Site) or SAC (Semi Anechoic Chamber).

A major problem with most of the open test sites is that the environment noise level (above all, the one caused by intentional transmitters) is so high that compliance testing is almost impossible. In this context 'high' means high compared to the emission limits for equipment under test (EUT) which have to be verified. The measurement is therefore almost impossible to carry out in practice. It is possible to measure the electric and magnetic fields very close to the EUT (where the disturbance field of the EUT is much higher) and estimate what its value if would be measured at the official distance (3,10,30 m). The estimate is burdensome, since at these frequencies and measurement distances we are always in the near field.

Within a few years the official measurements of magnetic field strength, will be carried out according to the 'van Veen method' applied to not too-large equipment, (Bergervoet and van Veen, 1989) [9]. The measurement distance is reduced to zero since the EUT is placed inside a loop antenna system (LSA) consisting of three mutually perpendicular large-loop antennas. The interference capability of the magnetic field of the EUT is then measured in terms of the currents induced in the Loop Antenna. The method with the LAS has several advantages: it is an indoor method, it has a very good induced signal to environment-noise ratio and it is a rapid method since neither the LAS nor the EUT has to be rotated during the measurements resulting in enormous savings of time and money. A disadvantage might be that the dimensions of the EUT which can be placed in the LAS are limited.

II. VAN VEEN LOOP ANTENNA

Van Veen (called also Van Veen/Bergervoet) loop antenna setup consists of a number of elements: the loops, the slits, the current probes, the coaxial switch, the ferrite absorbers and the calibration dipole; their requirement specifications are defined in [1] and [2]. The system is shown in Fig.l.

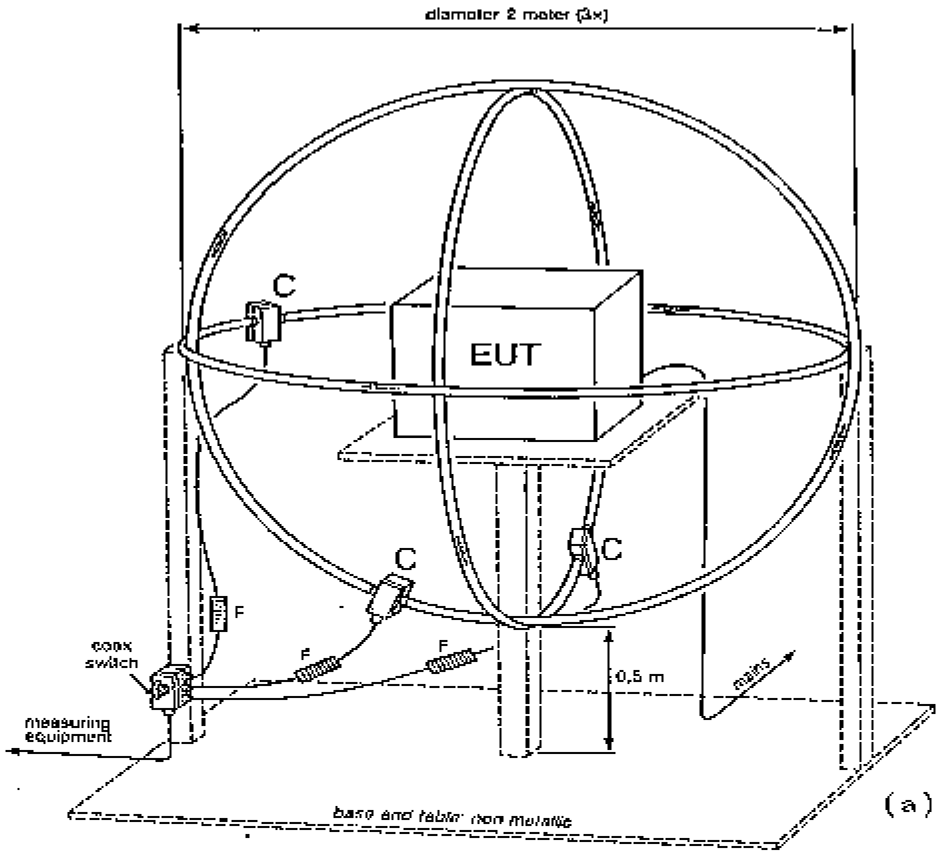

Fig. 1 Van Veen loop antenna [2].

The Van Veen antenna measures the magnetic dipole (magnetic field emissions) of the EUT as a vector quantity in X, Y and Z directions by means of three loops in the x, y and z planes as shown in Fig.2. Currents induced in the loops couple inductively into current probes and the corresponding output voltages can be analyzed using a spectrum analyzer for magnetic field disturbance analysis. Ferrite rings are applied to the output cables to eliminate common mode signals, and the calibration of the final system depends largely on the characteristics of the current probes (operating at l V/A).

The outside frame supporting the loops is made of a diamagnetic material such as wood. Best for the working ability of the antenna is if the antenna's sensitivity to an electric field is suppressed. For that purpose two electric field slits (gaps) are placed in the loop. The frequency response characteristic of the coaxial loop antenna with two gaps can obtain an almost flat response if the terminating resistances are chosen equal to the one of the characteristic cable impedance (Z=50 Ω).

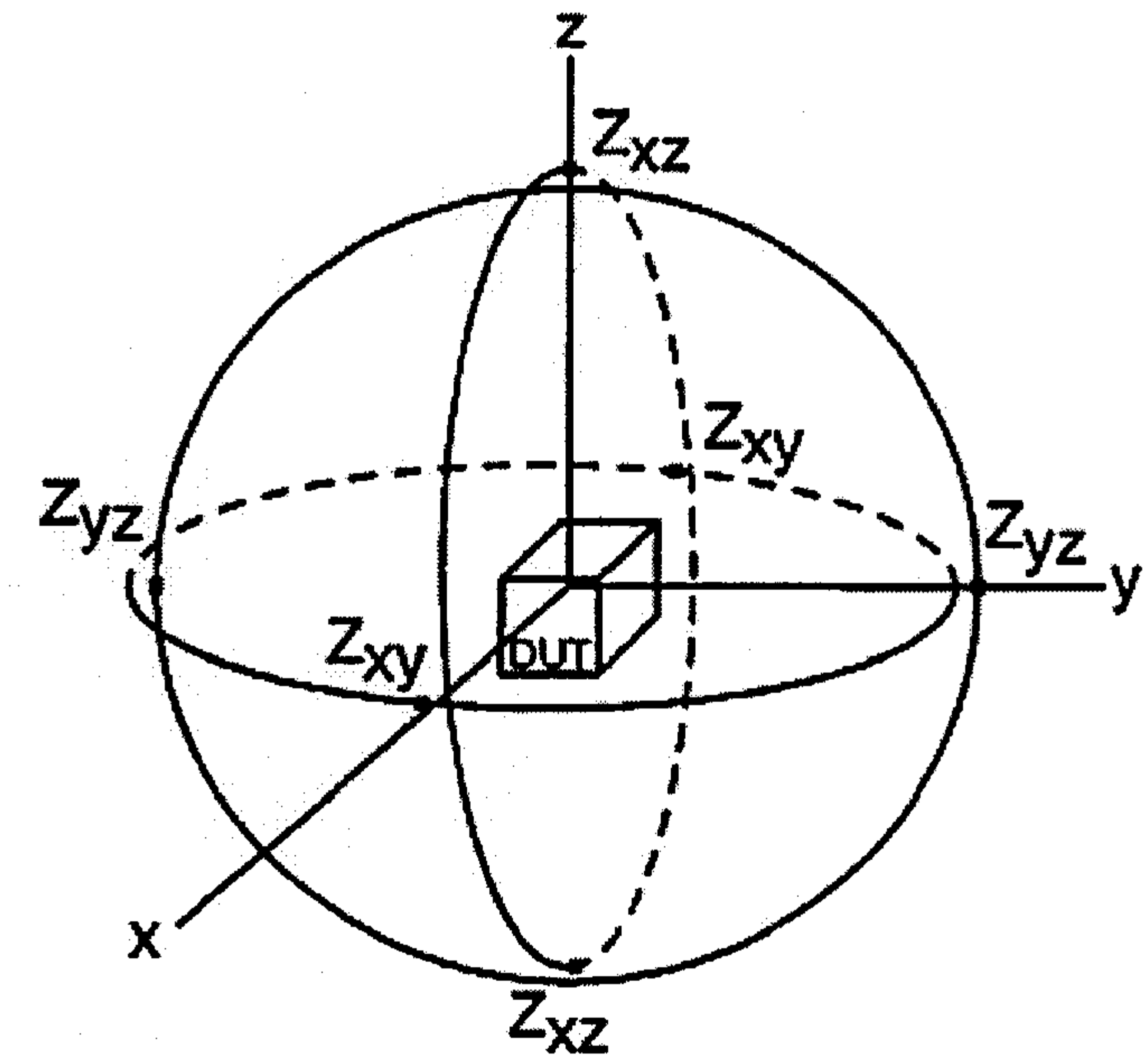

Fig. 2 Schematic view of a triplo loop antenna.

The loops of the Van Veen antenna should be comprised of coaxial cable (RG-223), enclosed and supported with conduit. With the EUT in position, a single turn in each loop should allow current measurements to be performed, with the aid of current probes, in each of the three directional planes. The operational frequency range of each of the three loops is between 9 kHz and 30 MHz.

The loops do not physically move, but are switchable between X, Y and Z planes by way of a coaxial switch. As the radius of the loops directly affects the operable frequency , range of the antenna, there are specific requirements relating to the size of each loop. In order to obtain a good spectral behavior for 9 kHz up to 30 MHz, the radius of a loop comprising two slits should not exceed 2.5m. A picture of the Van Veen Loop Antenna of the EMC laboratory of the University of Bologna is shown in Fig.3.

The current probes are connected to the coaxial switch and measuring receiver (spectrum analyzer) via RG-223 coaxial cable. This cable between coaxial switch and current probes is fitted with ferrite toroid to absorb any common mode signals (produced by Electromagnetic Interference EMI) that may affect magnetic field measurements. The transducer factor for each of the three current probes is required to be ± 2 dB for accurate response measurement. A calibration dipole is used as shown in Fig.4 to verify that the loops are properly working. The dipole must radiate electromagnetic waves over the frequency band of 9kHz to 30 MHz with the required frequency response shown in Fig. 5.

The measured current is sensible to eccentricity displacement and distance of DUT from the plane of the antenna; as a rule of thumb one can state that an accuracy of within 1 dB is obtained if the DUT is not moved out more than 30% of the antenna radius [9]. The magnetic field can be calculated at 3,10 or 30 m distance using the conversion factor between the induced current and the H field proposed in [9] and accepted by CISPR [1,2].

Two improvements on a LLAS are described in [13] to increase the available test space and to reduce the dependency on the field orientation. A similar method uses a double-loaded half-loop antenna placed perpendicular to a PEC surface to determinate radiated emissions from EUT [14].

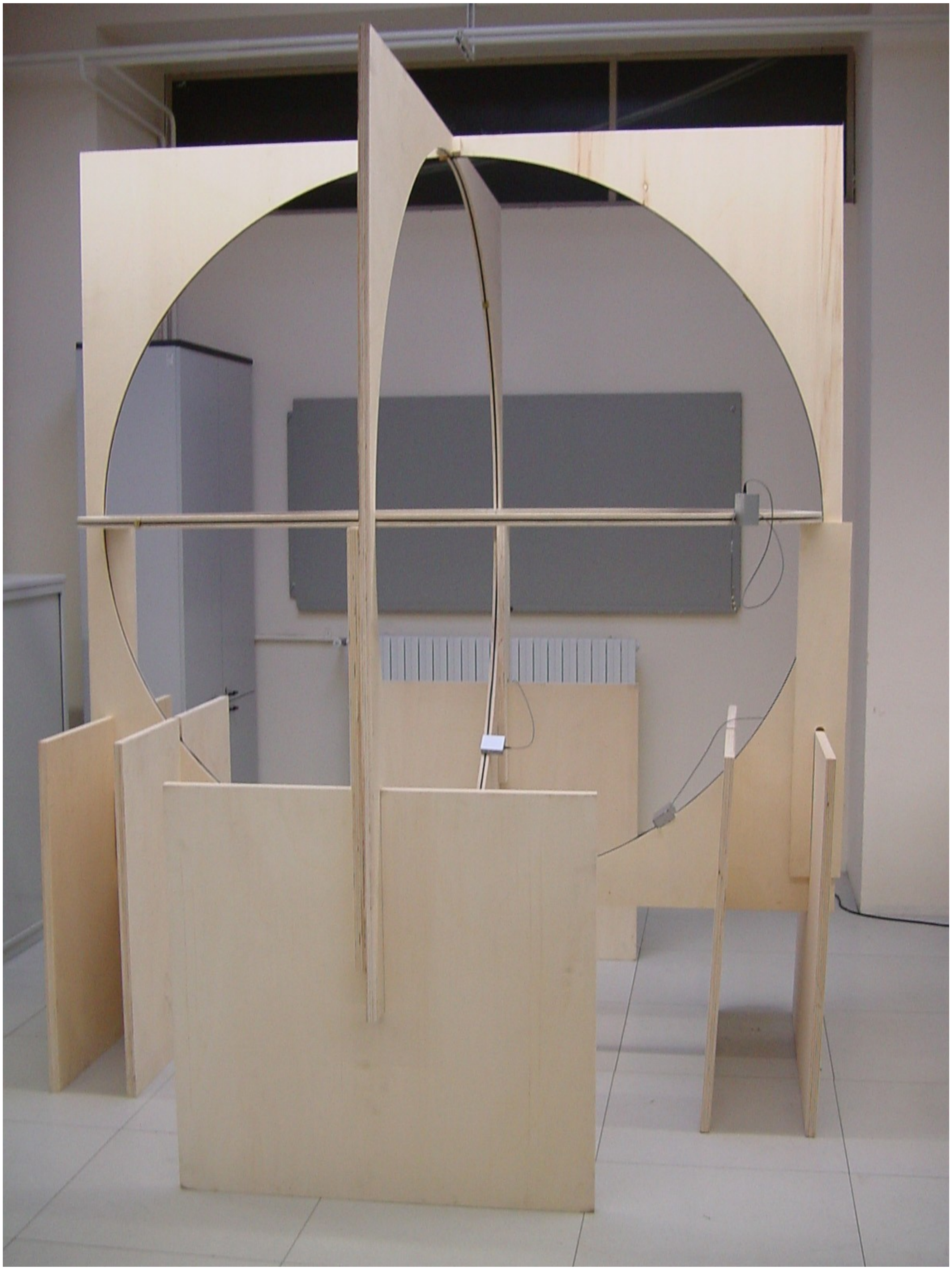

Fig. 3 Van Veen Loop Antenna of the EMC lab. of the University of Bologna.

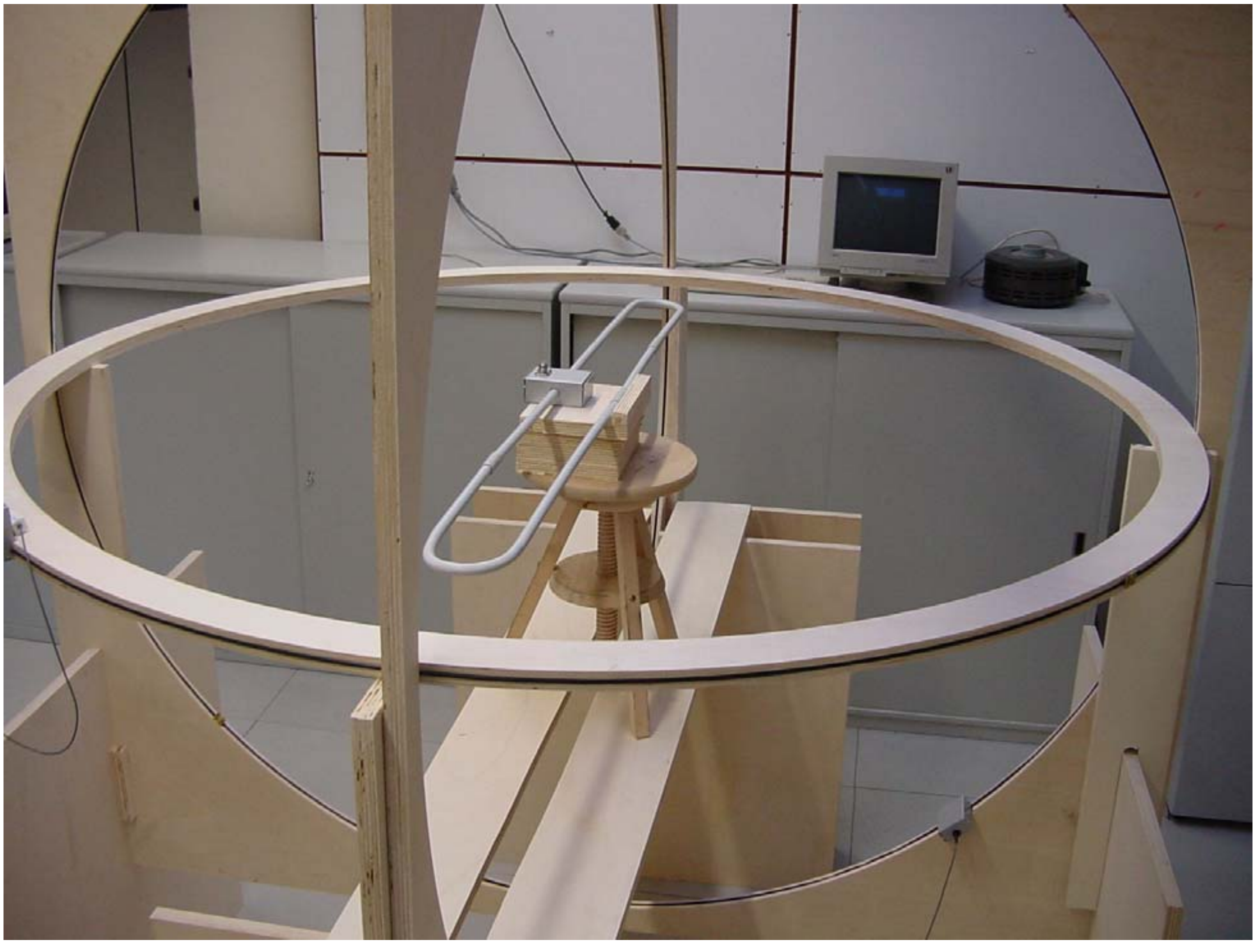

Fig. 4 Calibration of the Van Veen Loop Antenna

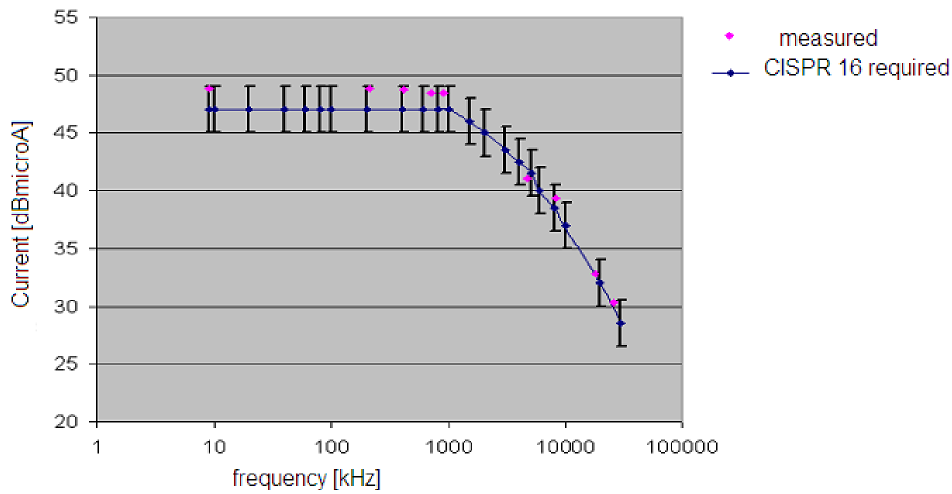

Fig. 5 Frequency response of the TLA to the calibration dipole.

III. THREE LOOP ANTENNA THEORY

For a single loop response to an incident plane wave, Kanda [6] indicates that it is possible to measure the magnetic loop and electric dipole currents using a loop antenna terminated with identical loads at two diametrically opposite points with a value of 270 Ω. After that, Kanda and Hill [7] have analyzed the response of a system of three orthogonal, concentric loops to a radiating dipole located at the center of the system. The radiating sources are assumed to be electrically small; therefore it can be characterized by equivalent electric and magnetic dipole moments. Fig.6 shows the geometry and coordinate system of a double gap loop of radius b and conductor radius a. The gaps are located at diametrically opposite points (ϕ=0,π) on the loop and are loaded with identical impedances Z_L.

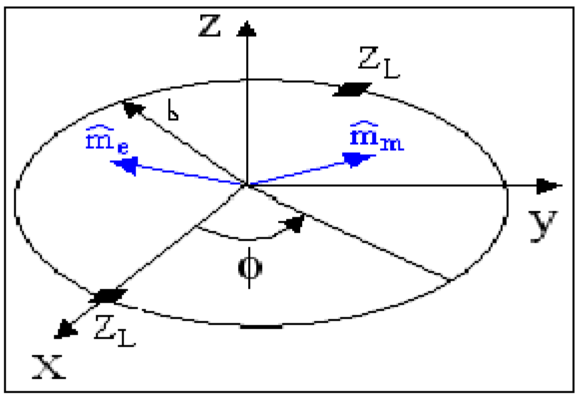

Fig. 6 A double gap loop loaded with identical impedances.

Equation Section 2

The electric and magnetic dipole moments are located at the origin of a rectangular coordinate system

$$\hat{\bar{m}}_e = \hat{m}_{ex}\overline{x} + \hat{m}_{ey}\overline{y} + \hat{m}_{ez}\overline{z} \qquad (2.1)$$

$$\hat{\bar{m}}_m = \hat{m}_{mx}\overline{x} + \hat{m}_{my}\overline{y} + \hat{m}_{mz}\overline{z} \qquad \mathbf{(2.2)}$$

The fields of electric and magnetic dipoles are well known [11] and the incident electric field E tangent to the loop can be expressed as

$$E^i_\phi(\phi) = A_0 + A_1\cos\phi + B_1\sin\phi \qquad (2.3)$$

where

$$A_0 = m_{mz}G_m \quad A_1 = m_{ey}G_e \quad B_1 = -m_{ex}G_e \qquad (2.4)$$

$$G_m = \frac{Z_w}{4\pi}\left(\frac{k^2}{b} - \frac{jk}{b^2}\right)e^{-jkb} \text{ and } G_e = \frac{-Z_w}{4\pi}\left(\frac{jk}{b} + \frac{1}{b^2} + \frac{1}{jkb^3}\right)e^{-jkb} \qquad (2.5)$$

Z_w is the free-space impedance, k is the free-space wave number.

If we follow Kanda's formulation and approximations [7], we obtain the following expression for the loop current

$$I(\phi) = 2\pi b E_0^i u(\phi) - I(0) Z_L v(\phi) - I(\pi) Z_L w(\phi) \qquad \textit{(2.6)}$$

$$u(\phi) = \frac{-j}{\pi Z_w}\left(\frac{A_0}{a_0} + \frac{A_1 \cos\phi}{a_1} + \frac{B_1 \sin\phi}{a_1}\right) \qquad \textit{(2.7)}$$

$$v(\phi) = \frac{-j}{\pi Z_w}\left(\frac{1}{a_0} + \frac{2\cos\phi}{a_1}\right) \qquad \textit{(2.8)}$$

$$w(\phi) = \frac{-j}{\pi Z_w}\left(\frac{1}{a_0} - \frac{2\cos\phi}{a_1}\right) \qquad \textit{(2.9)}$$

and a_0 and a_1 are defined in [7]. The derivation of (1.7),(1.8),(1.9) requires the loop to be not too large so that higher order Fourier components of the loop current can be neglected. The currents *I(0)* and *I(π)* can be determined from simultaneous equations obtained from (1.6) with ϕ=0 and π.

Assuming that a linearly polarized wave *E,* illuminates the loop from an orthogonal direction, we obtain the currents at the loads

$$I(0) = 2\pi b E_0\left(\frac{m_{mz} G_m Y_0}{1 + 2Y_0 Z_L} + \frac{m_{ey} G_e Y_1}{1 + 2Y_1 Z_L}\right) \qquad (2.10)$$

$$I(\pi) = 2\pi b E_0\left(\frac{m_{mz} G_m Y_0}{1 + 2Y_0 Z_L} - \frac{m_{ey} G_e Y_1}{1 + 2Y_1 Z_L}\right) \qquad (2.11)$$

where $Y_{0,1}$ are the admittances seen by the currents induced by the magnetic and electric fields. The quasi-static *(kb< 1)* forms of the admittances are given by

$$Y_0 \approx \frac{1}{jZ_w kb[Ln(\frac{8b}{a}) - 2]} \quad \text{and} \quad Y_1 \approx \frac{j2kb}{Z_w[Ln(\frac{8b}{a}) - 2]} \qquad (2.12)$$

By taking the sum and the difference of the currents, we obtain

$$I_\Sigma \equiv \frac{1}{2}[I(0) + I(\pi)] \approx 2\pi b E_0 \frac{m_{mz} G_m Y_0}{1 + 2Y_0 Z_L} \qquad (2.13)$$

and

$$I_\Delta \equiv \frac{1}{2}[I(0) - I(\pi)] \approx 2\pi b E_0 \frac{m_{ey} G_e Y_1}{1 + 2Y_1 Z_L} \qquad (2.14)$$

The sum current (1.12) depends only on the magnetic component of the plane wave expansion and the admittance seen by the current induced by the magnetic field and thus is proportional to the incident magnetic field. Correspondingly, the difference current (1.13) is proportional to the incident electric field.

To optimize the loop response for both the electric and magnetic fields, we equate the sum and difference currents, solve for the load impedance, and conclude:

$$Z_L \approx Z_w \frac{Ln(\frac{8b}{a})}{4} \tag{2.15}$$

The equation shows that the optimal loading point of the loop is independent of frequency and dependent only on the ratio of the loop and of the conductor radii.

We can solve (1.12) and (1.13) directly for the magnetic and electric dipole moments obtaining

$$m_{mz} = \frac{I_\Sigma(1+2Y_0 Z_L)}{2\pi b G_m Y_0} \text{ and } m_{ey} = \frac{I_\Delta(1+2Y_1 Z_L)}{2\pi b G_e Y_1} \tag{2.16}$$

Thus, the sum current can be used to measure the magnetic dipole moment, and the difference current can be used to measure the electric dipole moment. The other components of the dipole moments can be obtained in an analogous manner. The loop in the *xz* plane can be used to measure m_{my} and m_{ex},, and the loop in the *yz* plane can be used to measure m_{mx}, and m_{ez}. The total power P_T radiated by the source can be written in terms of the magnitudes of the six dipole moments [7].

$$P_T = \frac{40\pi^2}{\lambda^2}[\|m_e\|^2 + k^2\|m_e\|^2] \tag{2.17}$$

The expression for the power pattern is more complicated and involves not only the amplitudes but also the phases of the electric and magnetic dipole moments[12].

From the equivalent electric and magnetic dipoles of an EUT, the Electric and Magnetic field in far field can be calculated [11].

IV. OPTICALLY LINKED TRIPLE LOOP ANTENNA CONSTRUCTION

The antenna radius *b* was chosen as a compromise between a large loop which has high sensitivity and can accommodate a large test object and a small loop which will have a higher cutoff frequency. *b*= 0.5

m was the largest loop which could fit our size requirements and operates up to 100 MHz. The conductor radius *a* needs to be kept as small as possible to reduce field perturbations and surface RF current loops. The loops were built of 0.019 m OD copper tubing because easier to construct and less costly. The dimensions of the loop and equation (1.14) leads to an optimal Z_L of 315 Ω. We chose our load impedance at 290 Ω because the response of the loop is nearly identical for a loading impedance from 270 Ω to 400 Ω[6].To maintain the balanced configuration of the antennas and to prevent ground loops and field perturbations from any lead cables, we put an optical link between the gaps and the remote detector.

The design of the fiber optic links for each loop was driven by the antenna characteristics. Fig. 7 shows the block diagram of one loop of the TLAS.

Each transmitter detects one RF gap voltage (current), amplifies it, and modulates a LED. Each optical signal is split by a fiber coupler and detected by a pair of photodiodes in the receiver to create the appropriate sum and difference signals. The components in each loop are carefully matched so the phase and amplitude integrity of the signals are maintained.

The circuitry of the optical transmitters and their battery supplies is illustrated in Fig. 8.

The 1:1 balun (RF wideband transformer) ensures that the antenna remains in a balanced configuration and provides DC isolation between the two transmitter power supplies. The RF current injected into the base of the transistor is amplified and modulates the LED. By adjusting the potentiometer R2 in the base bias circuit, the bias current through the LED can be adjusted.

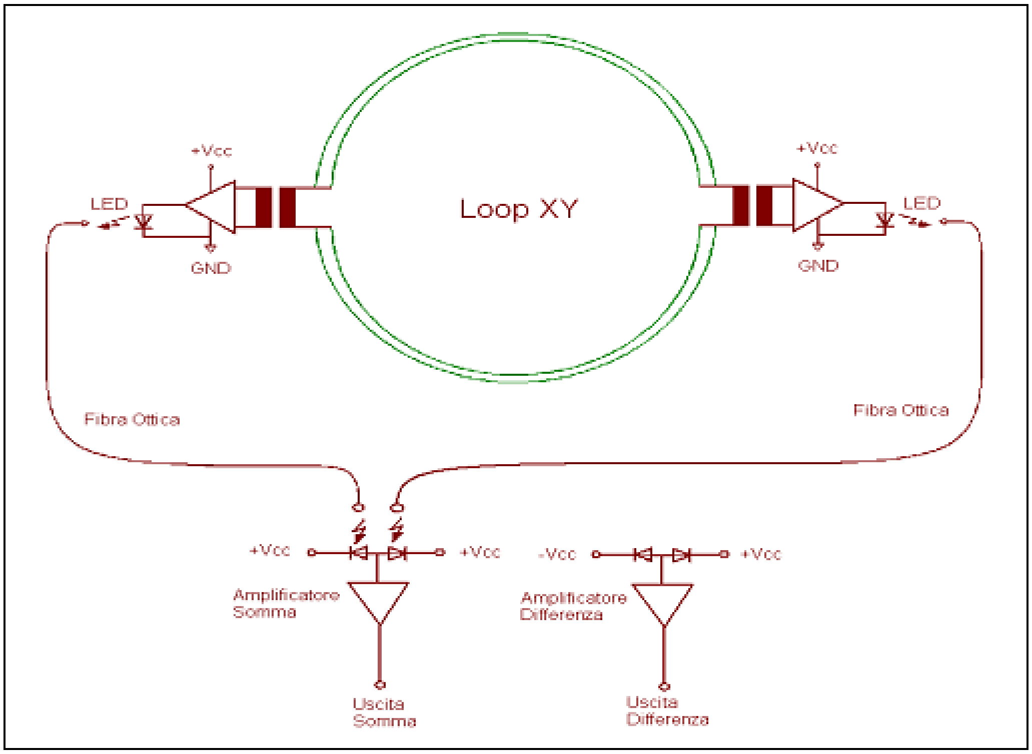

Fig. 7 Schematic view of TLS

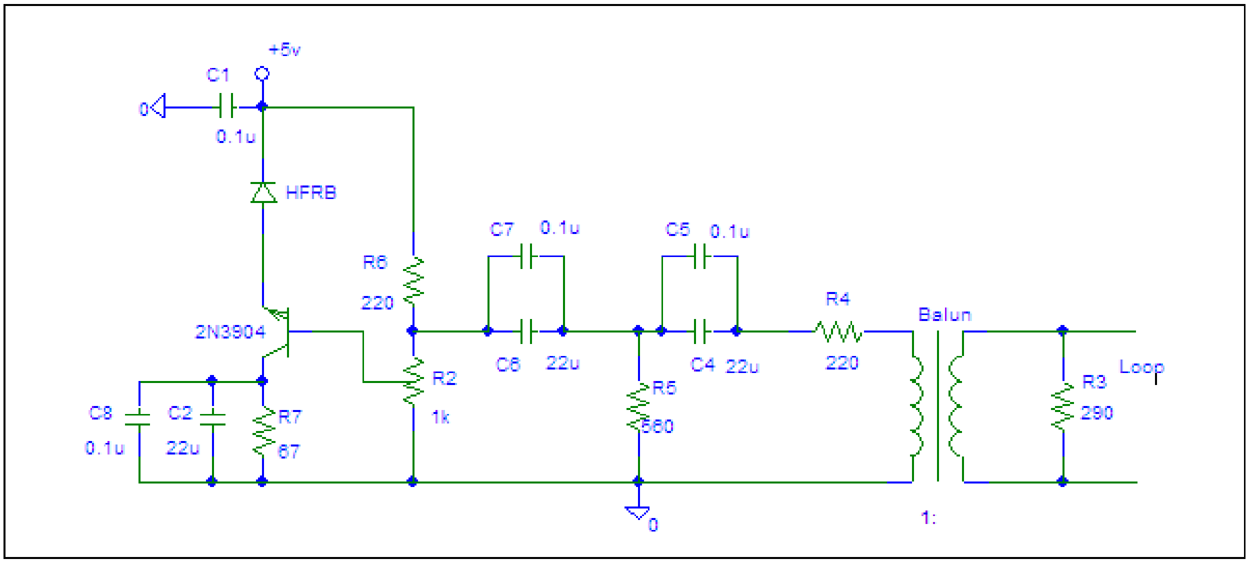

Fig. 8 Circuitry of the optical transmitter

The LED bias current was set so the diode HFRB operates in a nearly linear region for a reasonable range of field levels. The resistor *R4* was selected to match the RF impedance of the transistor to the optimal antenna loading impedance.

The optical signals are transmitted via a pair of well matched optical fibers to the receiver. The outputs from each coupler are detected in a way to form the sum and difference signals from each loop. The receiver is made of two independent circuits as shown in Figs. 9-10.

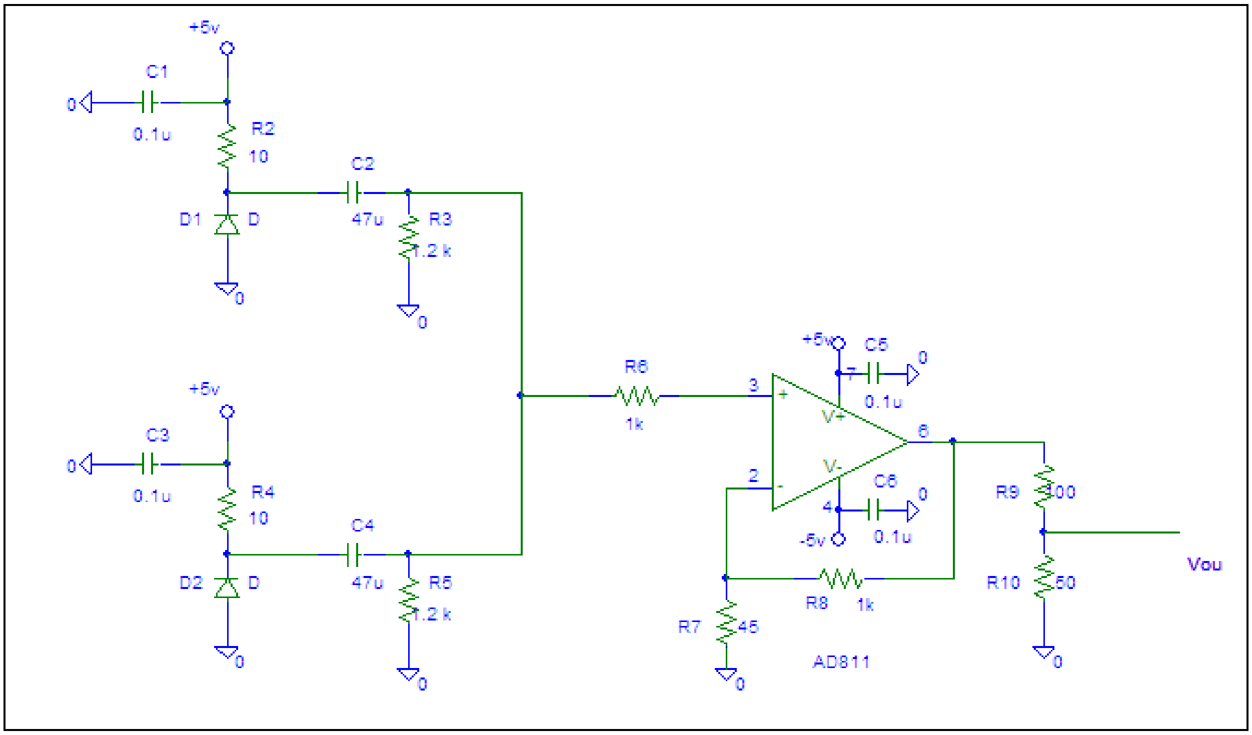

Fig. 9 Optical receiver and signals sum circuit.

In the sum circuit, the incident light in diodes *D1* and *D2* both sink RF current from the amplifier AD811 which yields a net sum of the currents as shown in Fig.9.

In the difference circuit, diode *D3* and *D4* sink RF current from the differential amplifier AD8130 so the output is proportional to the difference of the signals as shown in Fig.10. The AD811 is used to supply the output with a reasonable voltage level. A few decoupling capacitor are added to avoid auto oscillations of the circuits.

A few picture of the optically linked triplo loop antenna system are shown in Figs.11-13

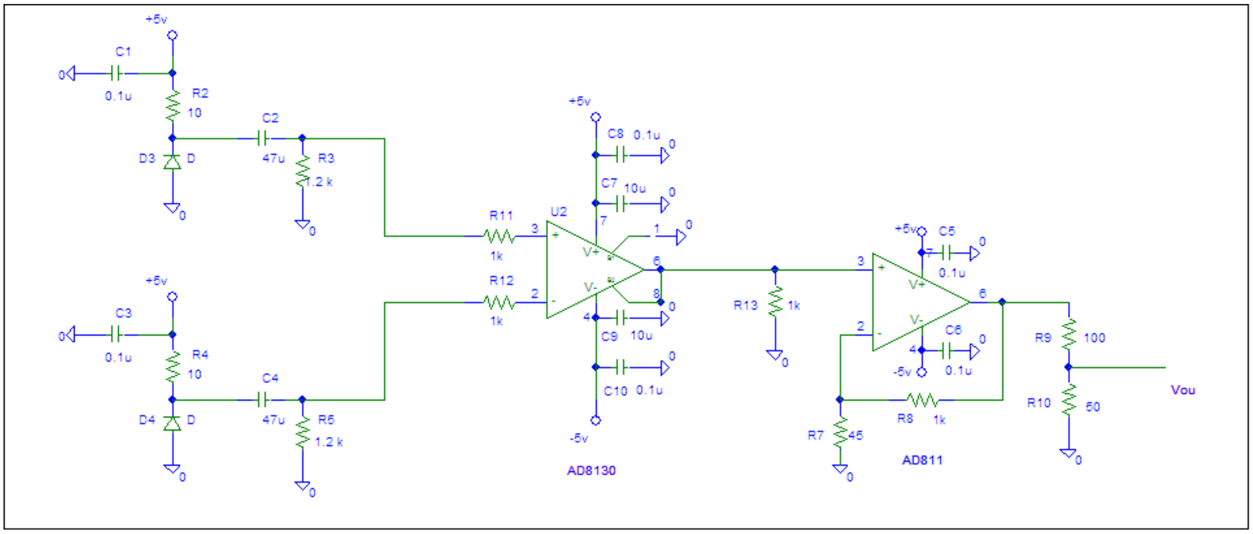

Fig. 10 Optical receiver and signals difference circuit.

Fig. 11 Optically linked Triple Loop Antenna in the EMC laboratory.

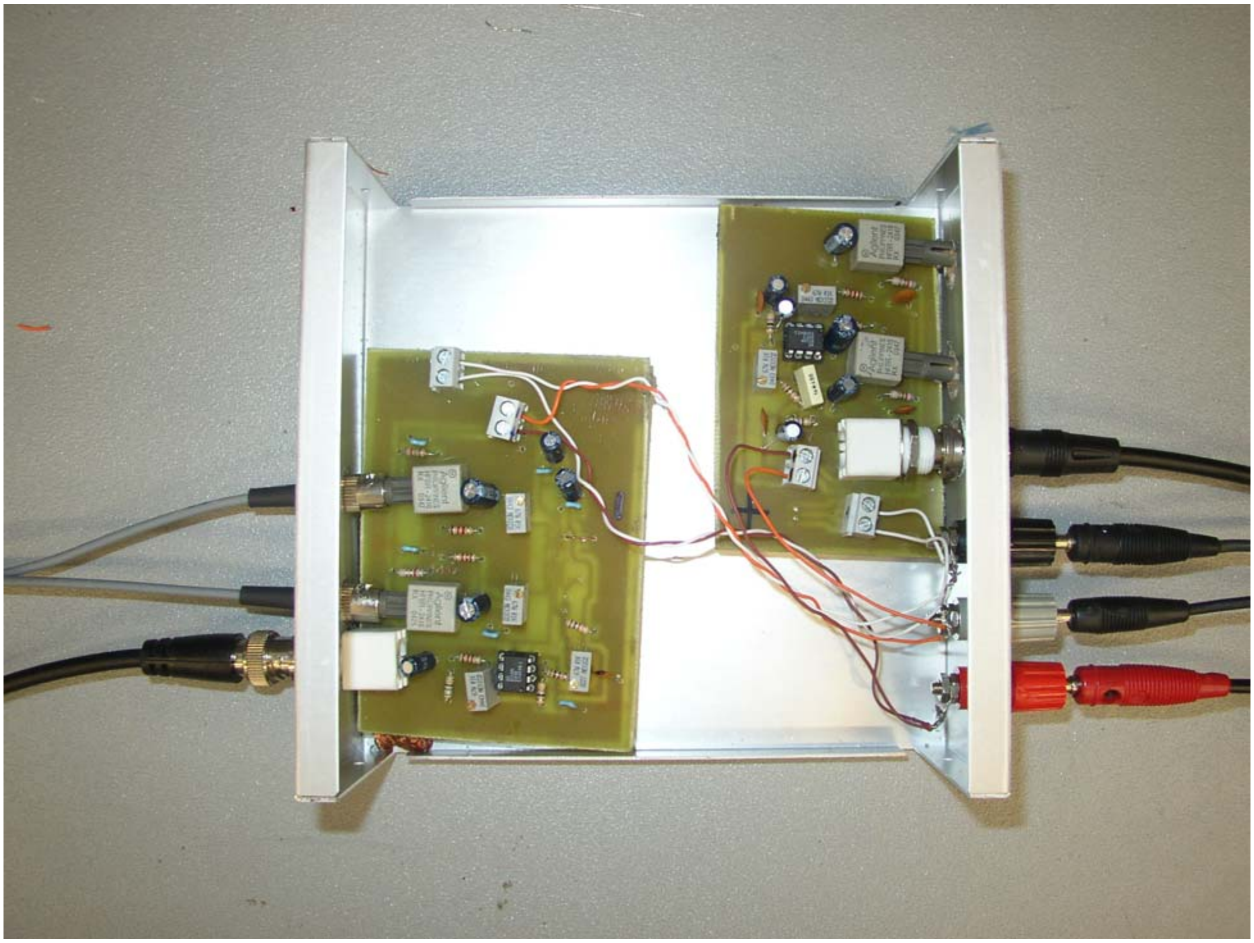

Fig. 12 Sum and difference signal circuits with optical receivers.

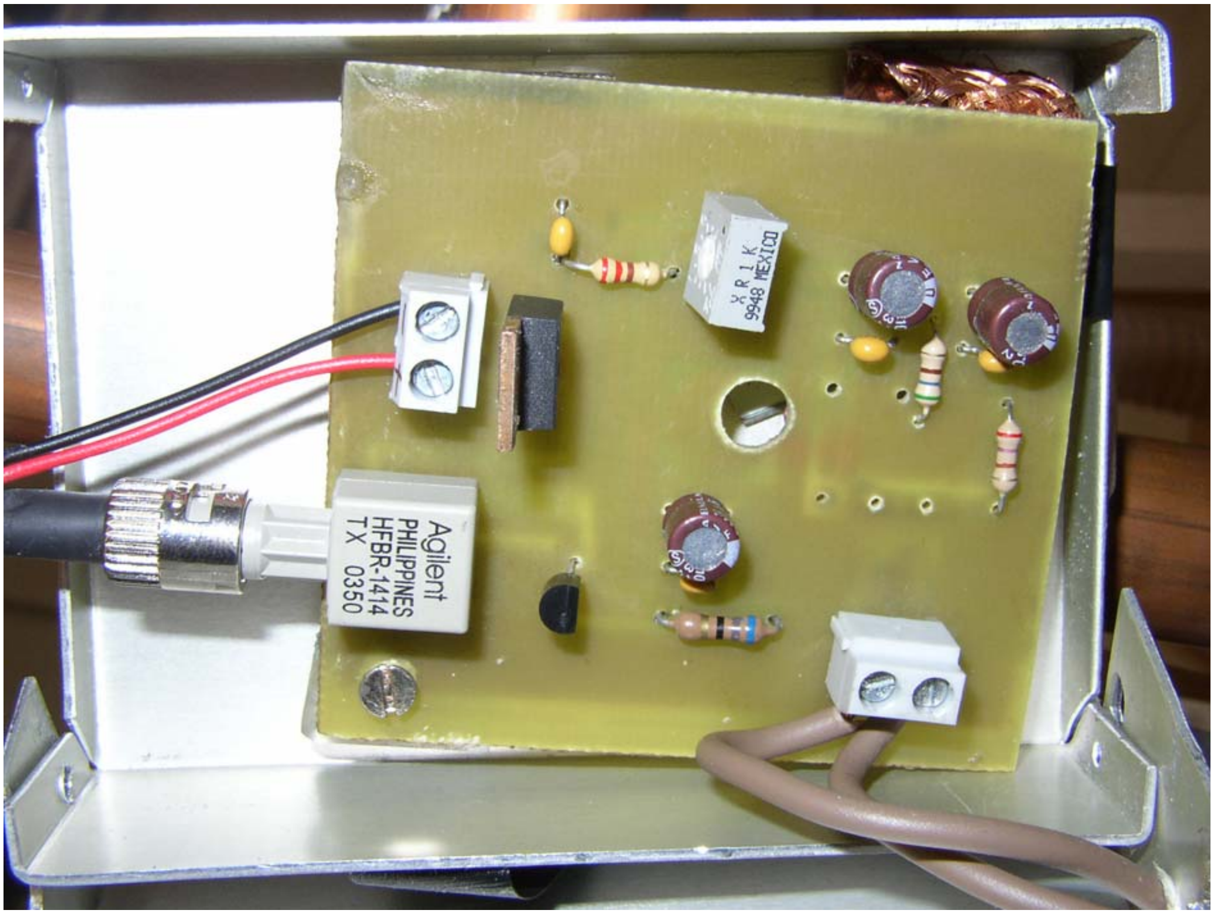

Fig.13 Optical transmitter connected to the TLA.

V. CALIBRATION OF A SINGLE LOOP

For each loop the two channels have been verified to present the same frequency response in ± 1 dB of accuracy all over the frequency range. The calibration is performed according to [8] and the antenna factor of a loop of the TLA is shown in Figs.13-14. The accuracy for the antenna factors in Figs. 13-14 is ± 2 dB all over the frequency range.

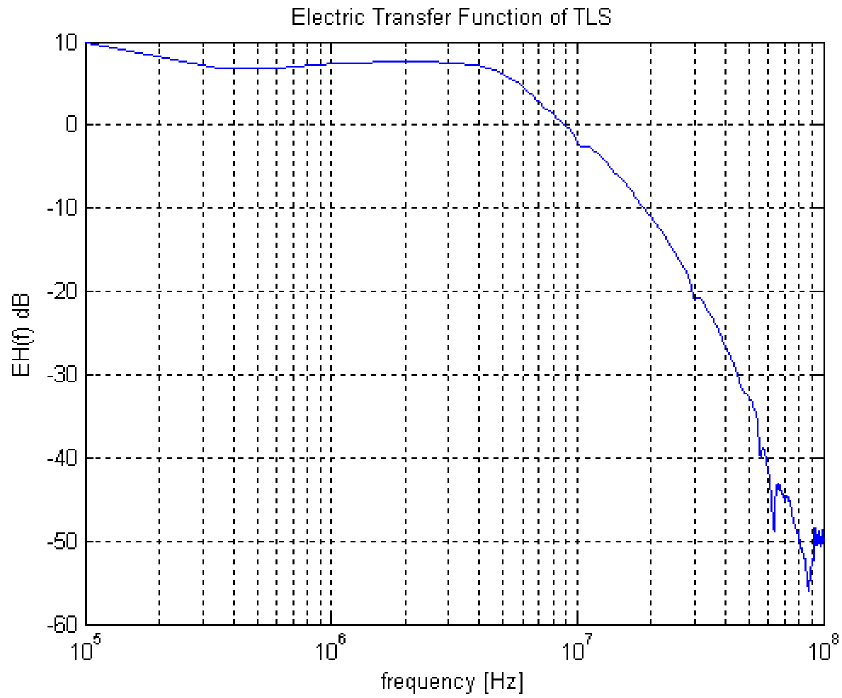

Fig. 13 Electric antenna factor for a loop of the TLA.

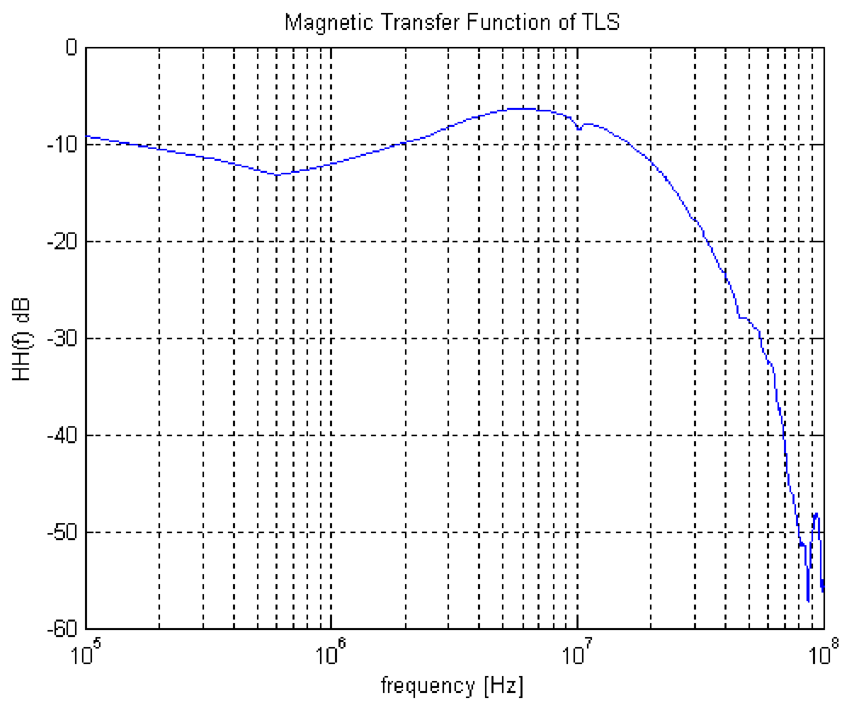

Fig. 14 Magnetic antenna factor for a loop of the TLA.

Chapter 3

A NEW MODEL FOR ESTIMATING DIGITAL CIRCUIT CURRENT WAVEFORMS

Yan Fu, Gian Lorenzo Giuliattini Burbui, and Todd Hubing
Dept. of Electrical and Computer Engineering
University of Missouri-Rolla

ABSTRACT

A resistance-inductance-capacitance (RLC) model is described for estimating current waveforms in digital CMOS circuits. The model is based on parameters that are readily derived from information available in board layout files and component data sheets or IBIS files. Compared with the simpler triangular waveform traditionally used to approximate current in CMOS circuits, the RLC model more accurately estimates the shape of the current waveform in the time domain and the amplitudes of the upper harmonics in the frequency domain.

I. INTRODUCTION

Estimating the radiated EM emissions or crosstalk due to signals on a printed circuit board requires an estimate of the signal current. Normally, more emphasis is placed on modeling and controlling the voltage waveform in digital circuits. For binary digital signals, the voltage waveform alternates between a high and low level. However the current waveform can look very different, particularly in CMOS circuits with a capacitive load. T. Van Doren introduced a simple triangular pulse waveform model for estimating power-bus noise currents in CMOS circuits for an expert system evaluating emissions from PCB designs [1], which is shown in Figure 1.

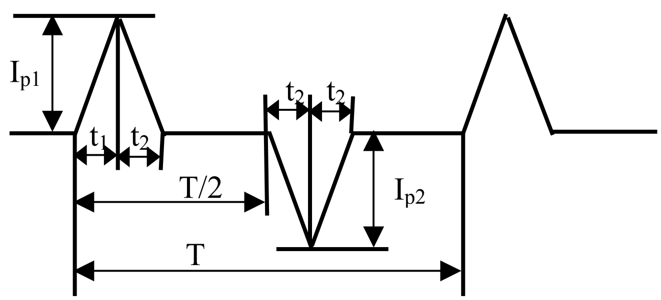

Fig. 1. Triangular model waveform for switching current.

J. Chen [2] and J. Mao [3] have applied this model to estimate power-bus noise due to multiple devices switching simultaneously. A similar model has been used by other researchers to estimate both signal and power currents [4]-[18]. For example, N. Na used a triangular waveform model to model core switching currents [8][10]; L. Bouhouch used a similar waveform to model controller I/O switching currents [9]; and Kriplani employed a triangular waveform to model capacitive load currents [15].

The triangular waveform model has the advantage that it is based only on the amplitude and risetime of the voltage waveform. These parameters are generally readily available. However, this simple model does not do a good job of estimating the amplitude of the upper harmonics that are often very important when trying to anticipate or model a radiated emissions problem. Furthermore, with the advent of IBIS models and better simulation tools, information about the source and load impedances is often readily available. This makes it possible to obtain reasonably accurate current waveforms directly from voltage waveforms.

This paper explores the possibility of replacing triangular waveform current estimates with estimates based on a series RLC model for CMOS circuits. Simple formulas are derived for the current based on parameters that are normally available or readily estimated for CMOS circuits. The paper is organized as follows: Section II discusses the derivation of the new model. In Section III, new model calculations are compared with SPICE simulations. In Section IV, the measured current spectrum from a test board is compared with the new model and triangular model calculations.

II. RLC MODEL

A. Calculation of the current spectrum I(f).

The transient current drawn from a CMOS IC by a nearby CMOS load can be estimated using an RLC series equivalent circuit as shown in Figure 2. The voltage source and resistance represent the Thevenin equivalent model for the CMOS source. L represents the connection inductance between the source and load. C is the input capacitance of the receiving device.

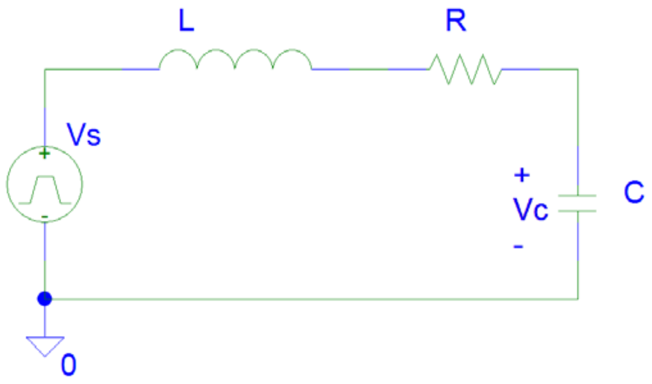

Fig. 2. Equivalent RLC circuit for a CMOS output gate and its load.

R can be obtained from IBIS voltage-current plots or estimated from the device data sheet as [19],

$$R \approx \frac{V_{CC} - V_{OH}}{I_{OUT}} \quad . \tag{1}$$

L depends on the geometry of the connection between the source and load. It can generally be estimated using simple closed-form formulas [20].

The voltage across the capacitor, V_C , can be determined by solving the second-order differential equation,

$$\frac{d^2V_C}{dt^2} + 2\xi\omega_n \frac{dV_C}{dt} + V_C = \omega_n{}^2 V_s \tag{2}$$

where ξ is the damping factor of the circuit,

$$\xi = \frac{1}{2Q} = {R_1} \Big/ {2\sqrt{L_1 / C_1}} \tag{3}$$

and ω_n is the intrinsic resonance angular frequency of the circuit,

$$\omega_n = \frac{1}{\sqrt{L_1 C_1}} \quad . \tag{4}$$

The load current is then given by

$$i_C = C\frac{dV_C}{dt}. \tag{5}$$

The step response of (5) is given by

$$i_C(t) = \begin{cases} \Delta V \dfrac{C_1\omega_n}{2\sqrt{\xi^2-1}}\left(e^{-(\xi-\sqrt{\xi^2-1})\omega_n t} - e^{-(\xi+\sqrt{\xi^2-1})\omega_n t}\right)\cdot u(t), & \xi>1,\text{ or } 0<Q<0.5 \\ \Delta V \dfrac{1}{L_1} t e^{-t/\omega_n} \cdot u(t), & \xi=1,\text{ or } Q=0.5 \\ \Delta V \dfrac{C_1\omega_n}{\sqrt{1-\xi^2}} e^{-\xi\omega_n t}\sin\sqrt{1-\xi^2}\,\omega_n t\cdot u(t), & \xi<1,\text{ or } Q>0.5 \end{cases} \tag{6}$$

where $u(t)$ is the unit step function and ΔV is the amplitude of the source. The spectrum of the load current can be expressed in a simple closed form,

$$I(f) = \frac{2\Delta V}{j\omega}\frac{1}{R_1 + j\omega L_1 + 1/j\omega C_1}. \tag{7}$$

If $0 < Q < 0.5$, the circuit is over-damped. Fig. 3 and Fig. 4 show the time-domain waveform and the spectrum of the load current of an overdamped RLC circuit respectively. In this case, the component values were R=30 ohms, L=10 nH and C=100 pF. ΔV was 1 volt.

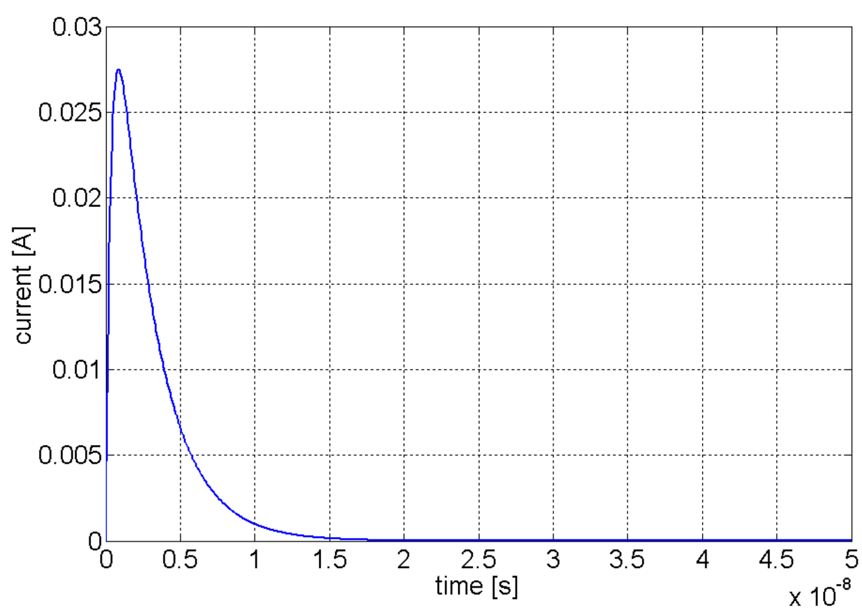

Fig. 3. Double exponential model in time domain ($0 < Q < 0.5$).

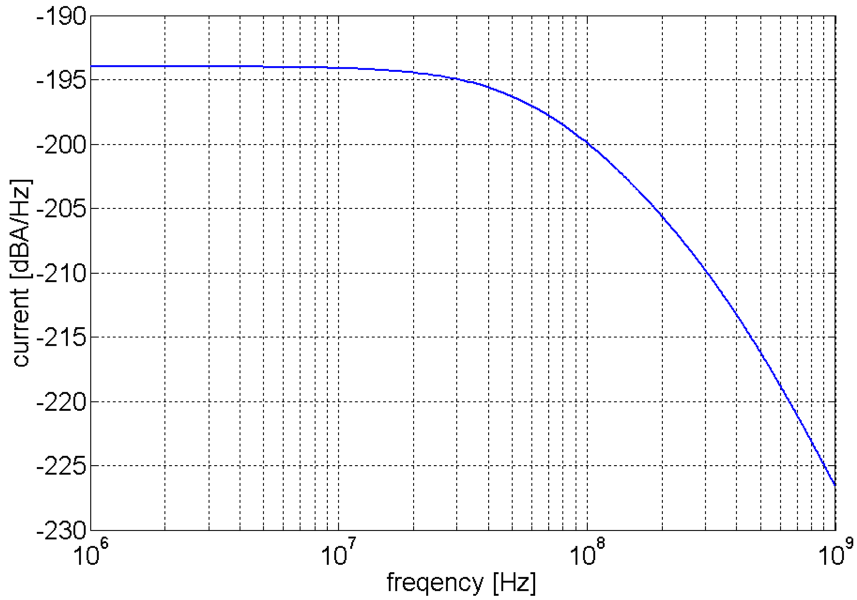

Fig. 4. Double exponential model spectrum ($0 < Q < 0.5$).

If $Q > 0.5$, the circuit is under-damped. An example of the current waveform and its spectrum for an underdamped circuit are shown in Fig's 5 and 6. In this case, the component values were R = 2 ohms, L = 10 nH and C = 100 pF. ΔV was 1 volt.

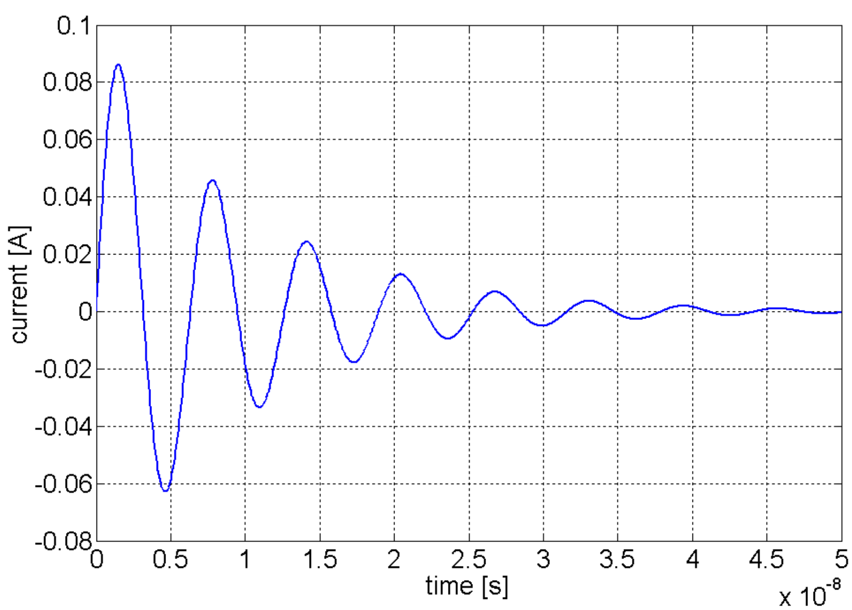

Fig. 5. Double exponential model in time domain ($Q > 0.5$).

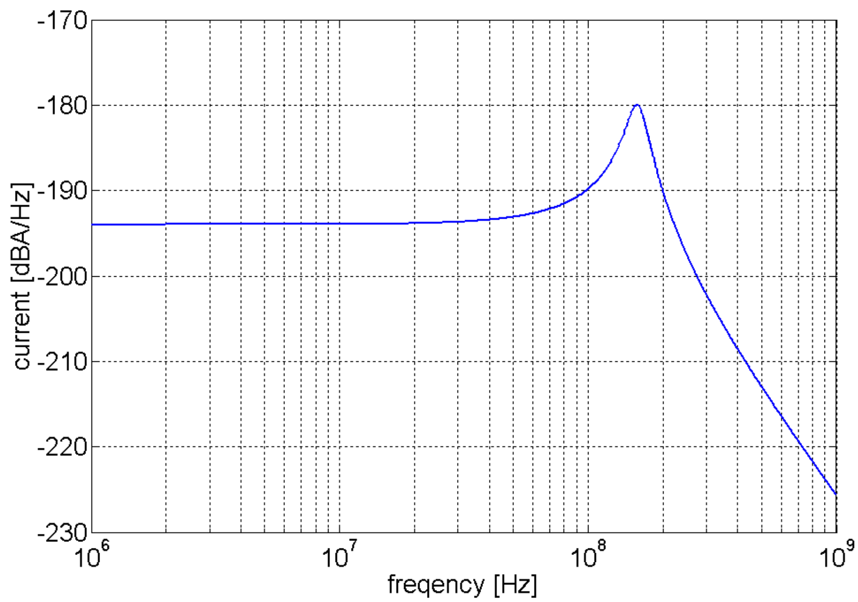

Fig. 6. Double exponential model spectrum ($Q > 0.5$).

When $Q = 0.5$, the circuit is critically-damped. An example of the current waveform and its spectrum for a critically-damped circuit are shown in Fig's 7 and 8. In this case, the component values were R = 20 ohms, L = 10 nH and C= 100 pF. ΔV was 1 volt.

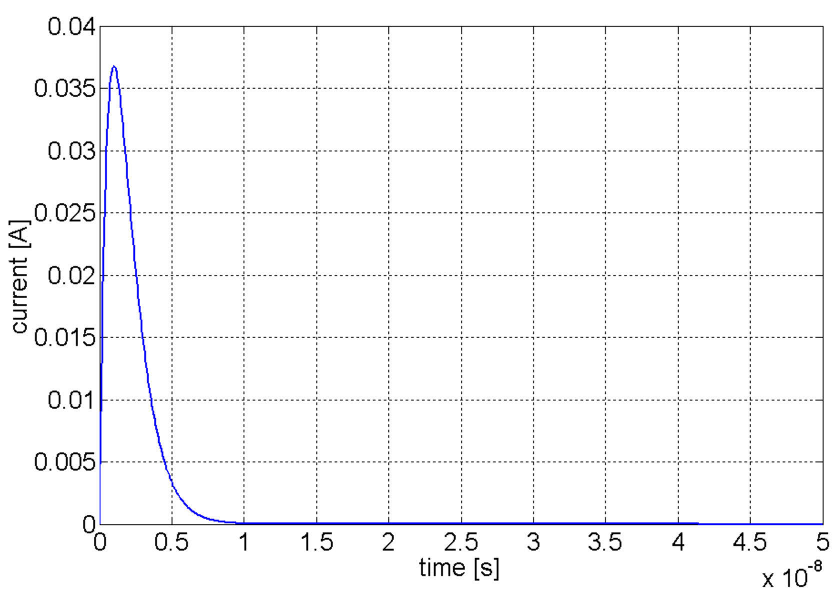

Fig. 7. Double exponential model in time domain ($Q = 0.5$).

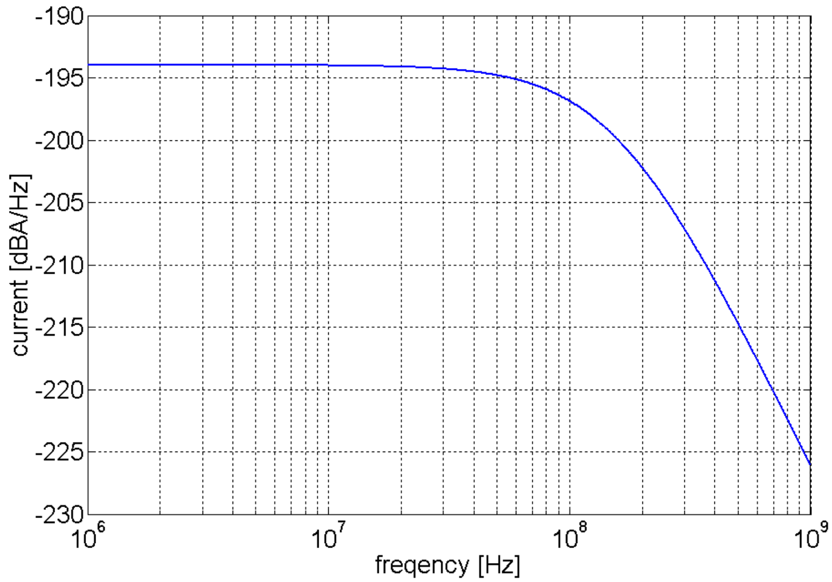

Fig. 8. Double exponential model in frequency domain ($Q = 0.5$).

B. Effect of finite source risetime

The transient current drawn by an IC device is also influenced by the source risetime. At high frequencies, finite risetimes cause harmonics of the source to fall off more rapidly. Practical models to estimate the current spectrum from CMOS sources above a few hundred MHz must take into account the finite risetime of the CMOS driver. The finite risetime of the voltage step supplying the RLC equivalent circuit can be accounted for in the frequency domain by simply multiplying by the source spectrum. For periodic trapezoidal waveforms, where T is the period of the voltage source and t_r is the rise and falltime of source; the magnitude of the current spectrum can be expressed as,

$$\left|I(nf_0)\right| = \frac{\left|V_S(nf_0)\right|}{\left|R_1 + j2\pi nf_0 L_1 + \frac{1}{j2\pi nf_0 C_1}\right|} \tag{8}$$

where f_0 is the fundamental frequency of the voltage source and $V_S(nf_0)$ is the magnitude of the source spectrum which is given by,

$$\left|V_S(nf_0)\right| = \begin{cases} \dfrac{2\Delta V}{n\pi}, & n \le \dfrac{T}{\pi t_r} \\ \dfrac{2\Delta V}{(n\pi)^2}\dfrac{T}{t_r}, & n > \dfrac{T}{\pi t_r} \end{cases} \tag{9}$$

where n is an odd integer ≥ 1. We can obtain expressions for the envelope of the load current and source voltage by replacing nf_0 with f in Equations (8) and (9) respectively,

$$|I(f)| = \frac{|V_S(f)|}{\left|R_1 + j2\pi f L_1 + \frac{1}{j2\pi f C_1}\right|} \tag{10}$$

$$|V_S(f)| = \begin{cases} \frac{2}{T}\frac{\Delta V}{\pi f}, & f \le \frac{1}{\pi t_r} \\ \frac{2}{T}\frac{\Delta V}{(\pi f)^2}\frac{1}{t_r}, & f > \frac{1}{\pi t_r} \end{cases}. \tag{11}$$

Generally, it is better to calculate the envelope (maximum value) when estimating currents for EMC calculations, because small variations in the duty cycle can have a significant effect on the amplitude of individual upper harmonics.

III. MODEL RESULTS VS. HSPICE SIMULATIONS

The formulas described in the previous section were validated using an HSPICE simulation tool to model the circuit in Fig. 2. Table 1 shows the parameters used for the simulations.

Table 1. Parameters used in the HSPICE simulations.

Parameters		Description	Value
t_r		Risetime of the voltage source	1 ns
Vcc		Amplitude of the voltage source	3.3 V
T		Pulse width of the voltage source	50 ns
T		Period of the voltage source	100 ns
L_1		Parasitic inductance	10 nH
C_1		Load capacitance	100 pF
R_1	Case 1	under damped	5 ohms
	Case 2	over damped	20 ohms
	Case 3	critically damped	50 ohms

Fig's 9 - 11 compare the simulated current spectra using HSPICE to the calculated current envelope obtained using Equations (10) and (11). Fig. 9 shows the case where the circuit is under-damped with a quality factor of 2. Fig. 10 shows the case where the circuit is critically damped. Fig. 11 shows the case where the circuit is over-damped, with a quality factor of 0.2. In each case, the model calculations accurately plot the envelope of the simulations. Both the HSPICE simulations and model calculations show that the envelope of the current spectrum has a slope of 60 dB/decade at high frequencies. This is due to the combined effects of the finite source risetime and the 40-dB/decade fall off of the LC circuit.

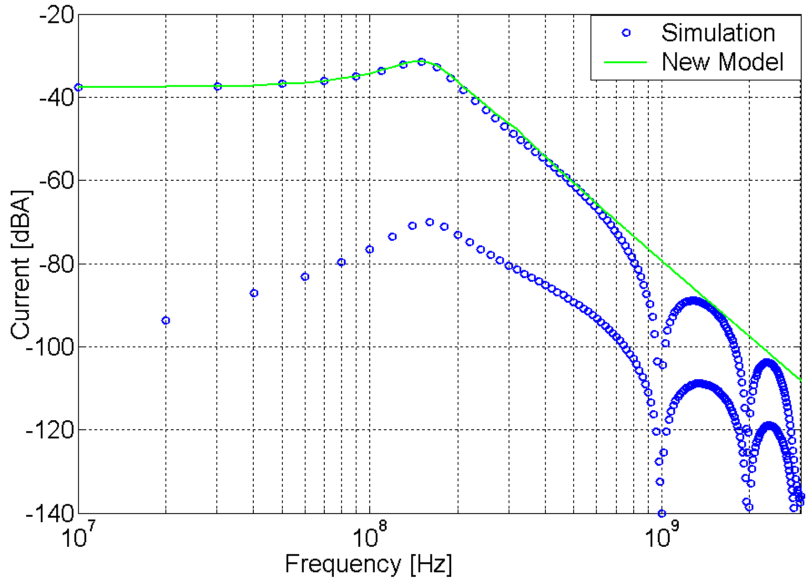

Fig. 9. Comparison of Spice simulation and new model calculation, Case 1: Q = 2.

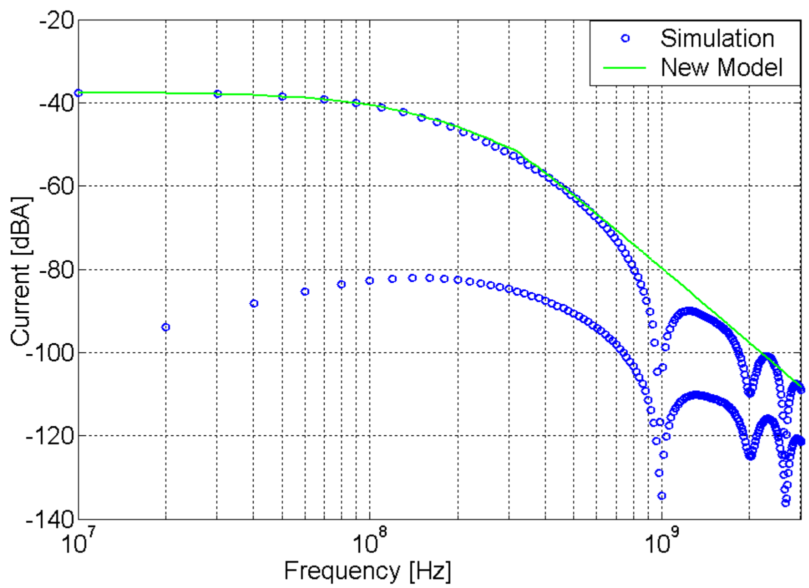

Fig. 10. Comparison of Spice simulation and new model calculation, Case 2: Q = 0.5.

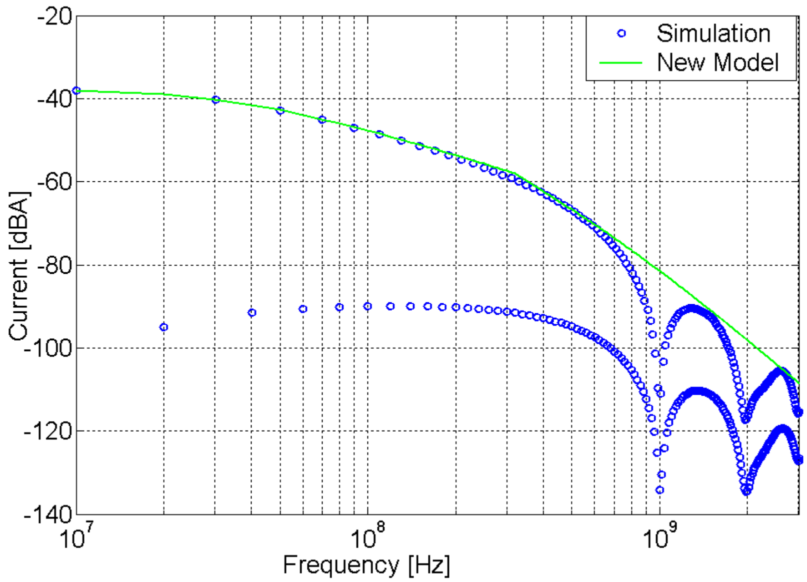

Fig. 11. Comparison of Spice simulation and new model calculation, Case 3: Q = 0.2.

IV. MODEL RESULTS VS. MEASUREMENTS AND TRIANGULAR APPROXIMATION RESULTS

A. Measurement Setup

The expression for maximum estimated current in Equations (10) and (11) was evaluated experimentally and compared to the triangular approximation. Fig. 12 shows the equivalent circuit used for these comparisons. A CMOS clock buffer was driven by a signal source (a 50-MHz oscillator) and was loaded with capacitors of different values. A 2-ohm resistor was connected in series with the load capacitor in order to measure the load current. The parasitic inductance of the load interconnect was about 10 nH. The turn-on resistance of the CMOS buffer was about 4 ohms; therefore the total series resistance was about 6 ohms. The circuit was implemented on a 7.6-cm by 5.0-cm six-layer circuit board.

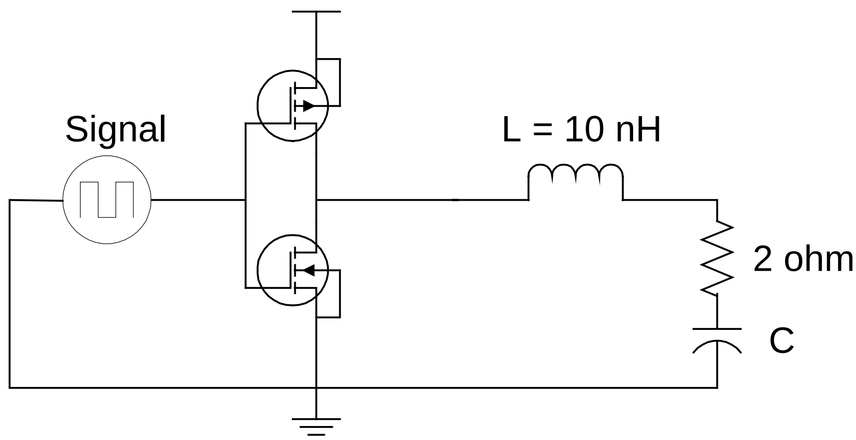

Fig. 12. Equivalent circuit of the measurement setup.

B. Results

1) Case 1. C = 10 pF.

Figure 13 shows the measured load current waveform (obtained by measuring the voltage across the 2-ohm resistor with an oscilloscope and dividing the voltage by 2-ohms) when the load capacitance was 10 pF. The quality factor of the circuit was about 5.3 (i.e. under damped). Fig. 14 shows the spectrum of the measurement (obtained using a spectrum analyzer) and envelope estimates obtained using Equations (10) and (11) and the triangular waveform model. The pulse width is approximated as a half of the ringing period in the triangular model calculation, $\Delta t = \pi\sqrt{LC}$. In the RLC model calculation, the risetime of the source signal ($t_r \approx 0.8$ ns) was obtained from an IBIS model [21]. The figure shows that the RLC calculation provides a better estimate of the envelope of the measured current spectrum than the triangular model. This is especially true at the upper harmonic frequencies. Fig. 14 shows that both the measurement and RLC model calculation show a 60-dB/decade slope at high frequencies, while the triangular model predicts a 40-dB/decade slope at high frequencies. The triangular model is not able to account for the combined effect of the finite source risetime and LC filtering.

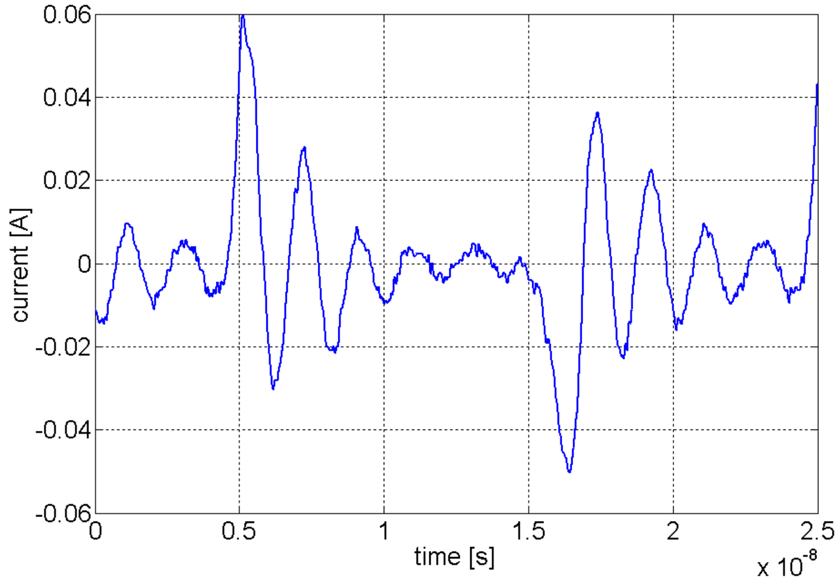

Fig. 13. Current waveform when C = 10 pF and R = 5 ohms.

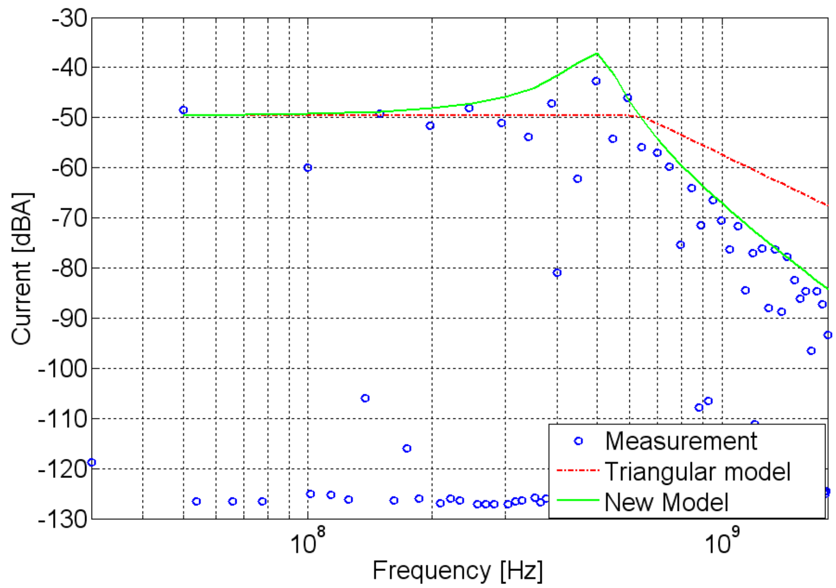

Fig. 14. Comparison of measurement, new model and triangular model calculation when C = 10 pF and R = 5 ohms.

2) Case 2. C = 100 pF.

Fig. 15 shows the measured current waveform when the load capacitance was 100 pF. In this case, the quality factor of the circuit was about 1.7 and the circuit was only slightly underdamped. Fig. 16 compares the measurement to the calculations using the RLC and triangular models. Again, the new model provides a better estimate of the envelope than the triangular model.

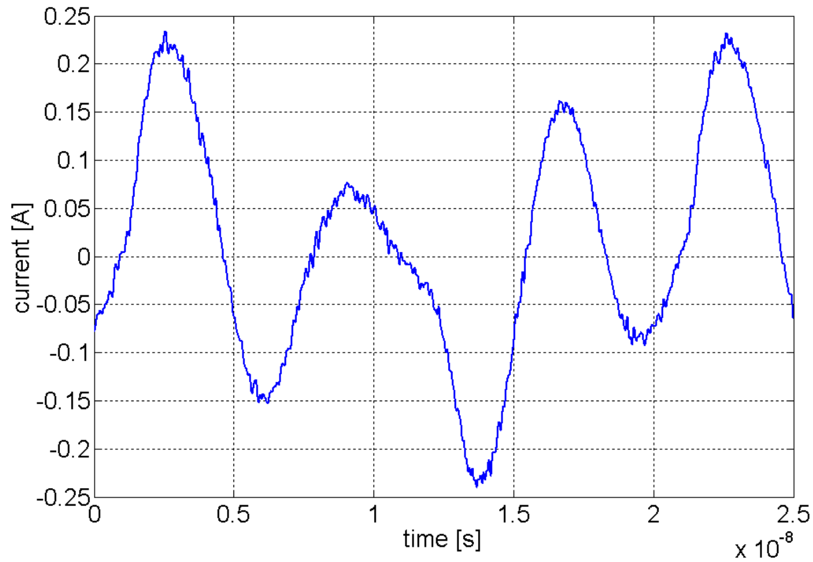

Fig. 15. Current waveform when C = 100 pF and R = 5 ohms.

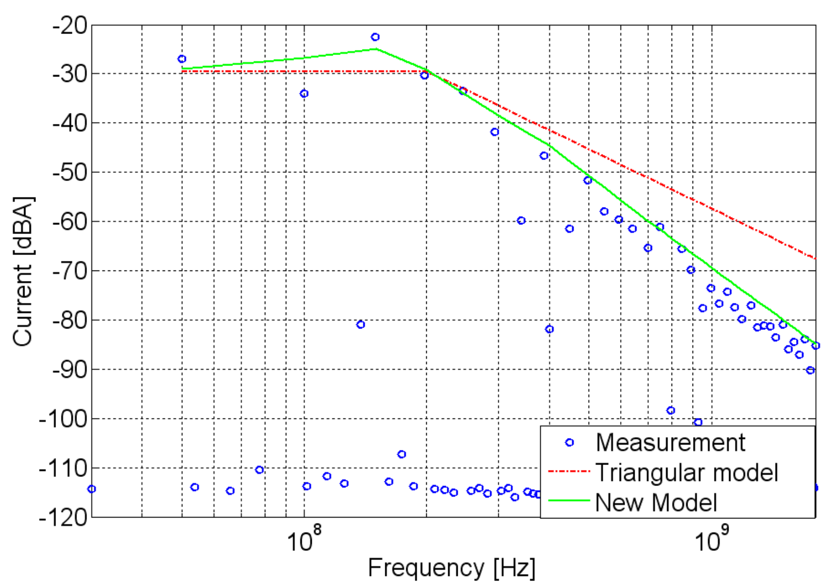

Fig. 16. Comparison of measurement, new model and triangular model calculation when C = 100 pF and R = 5 ohms.

3) Case 3: C = 10 pF, R = 100 ohms.

Figure 17 shows the measured current waveform when the load capacitance was 10 pF and the damping resistance was 100 ohms. In this case, the quality factor of the circuit was about 0.32. This is a slightly over-damped case. Figure 18 shows spectrum of the measurement and estimations using the RLC and triangular waveform models. For the triangular model, the risetime of the current was estimated as *2.2RC* (about 2.2 ns). The new model provides a better estimate of the envelope of the measured current spectrum than the triangular model estimation. The triangular estimate cut-off frequency is a little low, causing the upper harmonics to be under-estimated.

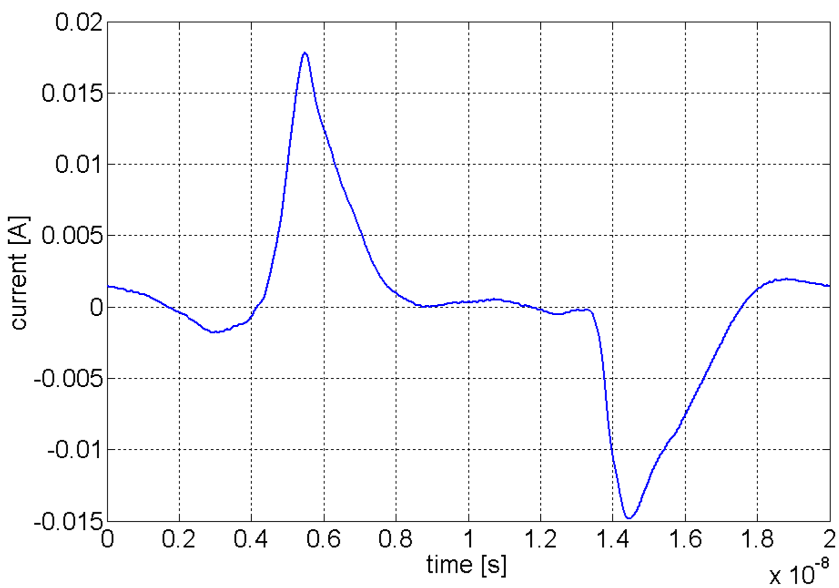

Fig. 17. Current waveform when C = 10 pF and R = 100 ohms.

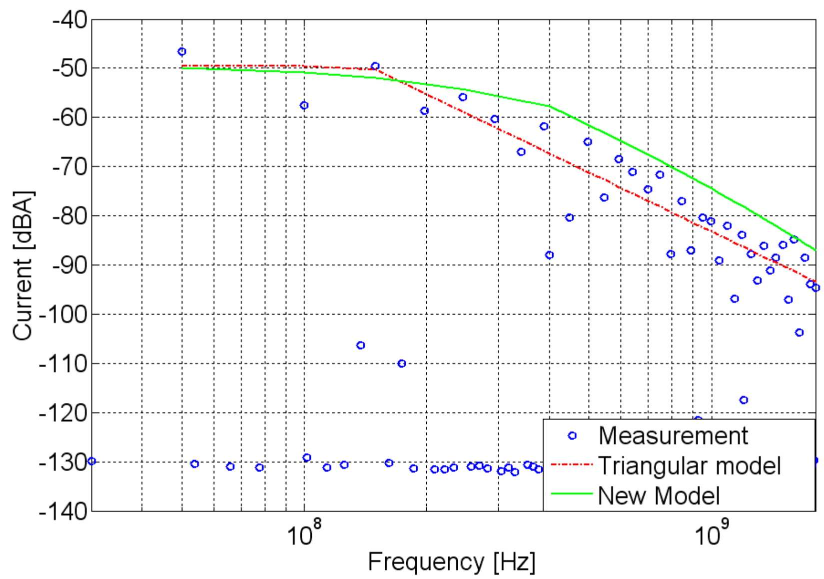

Fig. 18. Comparison of measurement, new model and triangular model calculation when C = 10 pF and R = 100 ohms.

4) Case 4: Current delivered to an active device.

The current delivered to an actual CMOS device was also measured. The Philips 74LCX16244 line driver IC has 16 outputs, which were connected in parallel and driven by another 74LCX16244 line driver IC. The input capacitance of each line driver (~ 7 pF) was obtained from the data sheet. Therefore, the total input capacitance of the buffer IC was about 112 pF. The interconnect inductance associated with the trace between the driver and receiver was estimated to be 6 nH using the technique described in [20]. The total resistance was about 16 ohms. In this case, the quality factor of the circuit was about 0.45. Figure 19 shows the current waveform. Figure 20 shows spectrum of the measurement and estimates of the envelope obtained using the RLC and triangular waveform models. For the triangular model, the risetime of the current was estimated as *2.2RC* (about 4 ns). The RLC model provides a better estimate of the envelope of the measured current spectrum than the triangular model estimation.

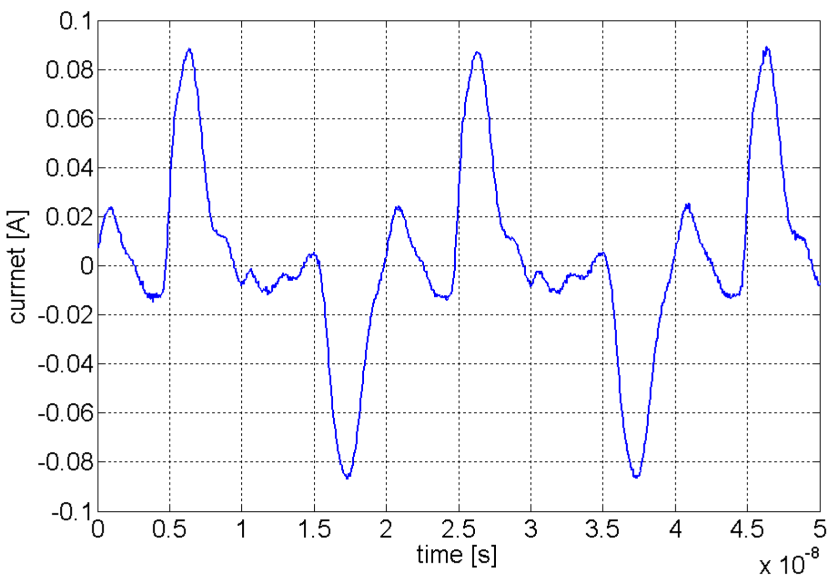

Fig. 19. Current waveform for an active device.

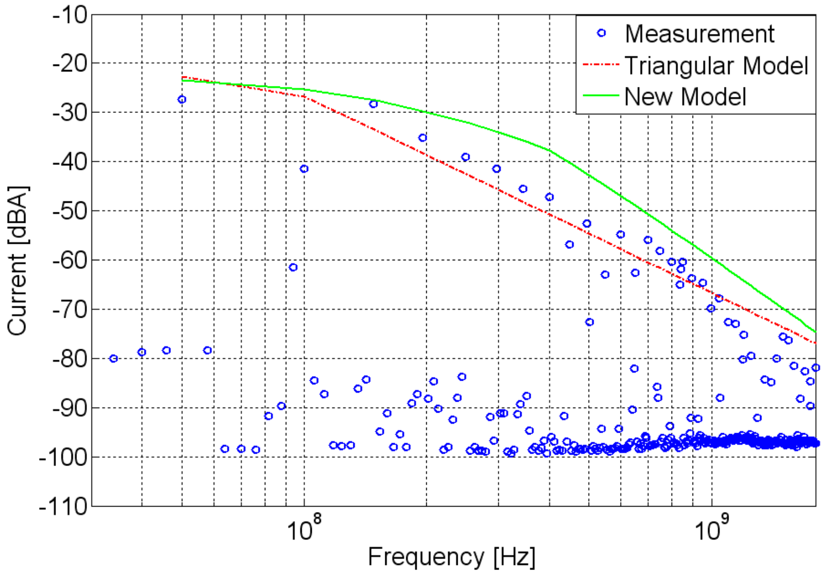

Fig. 20. Comparison of measurement, new model and triangular model calculation for active device current when C = 112 pF, L = 6 nH and R = 16 ohms.

V. CONCLUSIONS

The current spectrum calculated using closed-form formulas based on an RLC model was compared to simulations, measurements and triangular waveform model results. The RLC model provides a better estimate of the current spectrum than the triangular model, especially at upper harmonics. The RLC model predicts the 60dB/decade fall-off of the upper harmonics shown in both simulations and measurements, while the triangular model predicts a 40-dB/decade fall-off. Parameters required for the RLC model calculations are readily obtained from information available in board layout files and component data sheets or IBIS files.